Mathematical Modelling of Weld Phenomena 5; Eds. H. Cerjak,
H.K.D.H. Bhadeshia; Institute of Materials; London, UK, 2000.

ESTIMATION OF THE CHARACTERISTIC PROPERTIES OF THE WELD POOL DURING HIGH PRODUCTIVITY ARC WELDING

Patricio F. Mendez and Thomas W. Eagar
Massachussetts Institute of Technology
Cambridge, MA 02139

ABSTRACT

A new methodology for studying complex engineering problems is described. It permits one to obtain an estimation of the characteristic properties, driving forces, and effects in a system without a detailed solution of the actual governing equations. In employing this technique, it is necessary to write down the system of equations that describe the problem and to have insights into the physics of the problem. Through the simultaneous use of dimensional analysis and asymptotic considerations, the original system of differential equations (not necessarily linear) yields another set of equations, the latter involving only linear algebraic equations, which are significantly easier to solve. This method enables one to systematically solve problems that are very challenging with either dimensional analysis or analysis of differential equations alone. It is especially useful for problems such as welding, in which many driving forces act simultaneously, and it is not obvious which ones are dominant. Using this technique it is demonstrated and quantified for the first time that at high current and speed (when the weld pool surface is very depressed) the weld pool turns into a thin liquid film, and the arc shear force dominates over the Marangoni (thermocapillary), electromagnetic, and capillary forces.

INTRODUCTION

The suppression of welding defects and the increase of welding productivity have significant economic impact. Defects such as humping, undercutting, split bead or tunnel porosity constitute limits to welding productivity. These defects are generated in the weld pool, and in order to control them it is necessary to understand the fluid flow and transport processes in the molten metal.

The appearance of defects mentioned above is associated with the large depression of the weld pool observed at high currents and velocities. Bradstreet[1] studied humping formation in GMAW, and associated it with the presence of an "arc crater" where the surface of the weld pool was very depressed. Yamamoto and Shimada[2, 3] performed research on GTAW at low pressure, and concluded that the onset of humping was related to a transition in which the weld pool turned into a thin film under the arc. Savage *et al.* [4] also studied the formation of defects in GTAW and determined experimentally a relationship between the presence of defects at atmospheric pressure and welding current and speed. The occurrence of defects in the weld

pool depends mainly on the welding current and travel speed, as shown in the process maps of Figure 1.

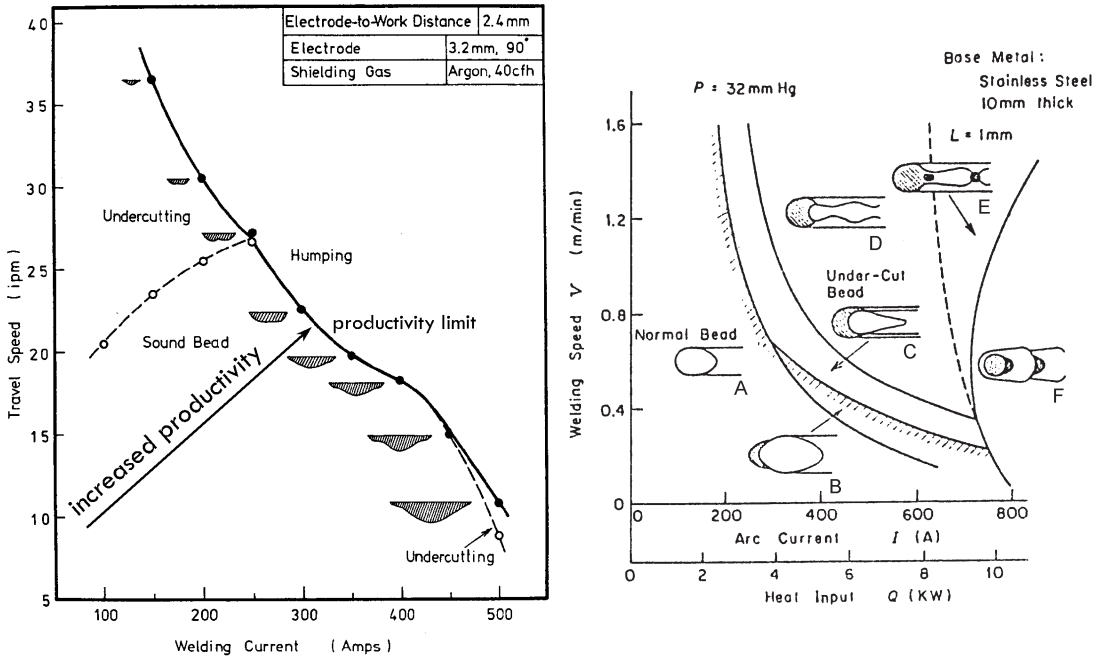

Figure 1: Process maps for GTAW. When the travel speed or welding current are too high, defects occur. The figure on the left corresponds to atmospheric pressure, after Savage *et al.* [4], the one of the right corresponds to 0.04 atm, after Shimada *et al.* [3]. In this last figure, each region contains a particular type of weld bead. Type A is a normal weld pool, with little surface depression. Type B is a sound weld, but the front of the weld pool is being "gouged". Type C has more severe gouging and produces an undercut weld. Type D presents two parallel humped beads at the side of the welds, and a "dry" path in between them. Type E is similar to type D, but the parallel beads collapse into each other, sometimes leading to tunnelling. Type F presents "dry" spots in between humps.

Previous research (summarized in Table 1) indicates four possible causes for the observed deep weld pool surface depression:

- Marangoni forces
- electromagnetic forces
- arc pressure
- gas shear on the surface

Marangoni forces are dominant at lower currents (under 200 A) where the weld pool presents recirculating flows, as determined by Heiple and Roper[5], Oreper and Szekely[6], and others. In this regime, electromagnetic forces increase with the welding current; they are not negligible at currents close to 200 A, and could possibly dominate the flows at higher currents. The arc pressure and gas shear act over the free surface affecting the properties of the weld pool, as

observed by Ishizaki[7], Choo and Szekely[8], Weiss *et al.*[9], and others. These forces increase with the welding current, therefore they could potentially be the dominant forces at high currents. Because of the difficulty of studying the weld pool in the high productivity regime, there has been no agreement in the past about which is actually the dominant force.

Table 1 summarizes the studies performed on deformation of the free surface of the weld pool. It shows that the early studies of weld pool surface depression were experimental, and included the major feature of the real weld pool at high currents: a gouging region (a region where the weld pool turns into a thin liquid film). A numerical model of weld pool surface deformation was presented by Friedman[10] in the late 1970's for small deformations. The analytical part of these works considers only arc pressure, capillary and hydrostatic forces, neglecting gas shear, Marangoni, and electromagnetic forces.

As greater computer power became available in the early 1980's, researchers attempted to model the welding process including more complex driving forces. Oreper and Szekely built the earliest numerical models of spot GTAW assuming a flat and rigid free surface[11, 6]. Only in the late 1980's was the simultaneous modeling of fluid flow and free surface in GTAW attempted by Zacharia *et al.*[12, 13].

Table 1 shows that the maximum current considered in numerical models of GTAW seldom exceeds 150A. This is because the larger surface deformation caused by higher currents significantly increases the complexity of the problem; it also makes the convergence of numerical methods very difficult. Na *et al.*[14] considered a current of 300A in 1992, but his later work does not exceed 200A. The newest numerical models of GMAW reach higher current values, of the order of 300A, but still far from the values used in practice for high productivity welding ($\approx$ 500A). Weiss[9] is the only one to have studied very depressed weld pools, focusing on the capillary forces during vertical welding, neglecting the effects of fluid flow.

Weld Pool Geometry At High Current

Figure 2 shows top, cross and longitudinal views of a GTA weld produced at high current and travel speed; Figure 3 shows a schematic of a weld pool in that regime. The most salient feature is the deep depression of the free surface, exhibiting a "gouging region" under the arc, a "rim" around it, and a bulk of molten metal at the rear of the weld pool. The gouging region is actually a very thin layer of liquid that follows the irregularities of the mushy zone, thus not reflecting light as a smooth surface. There are no recirculating flows due to the thinness of this region. The rim around the gouging region is a thicker liquid portion that transports molten metal to the trailing region at the rear of the weld pool. The transition line delimits the sharp transition between the gouging region and the trailing region. It is observed experimentally that this line moves toward the rear as the current increases[7, 3]. The elements of the weld pool present different configurations depending on the welding parameters. These variations are the origin of defects such as humping, undercutting, tunnelling, and split bead. It can be seen in Figure 2 that the cross section of a good weld shows no obvious signs of the very depressed surface that occurs during the melting process.

Methodology

In order to understand the transport processes acting on the weld pool at high currents and their relative importance, a particular scaling methodology (order of magnitude scaling) is used here. Scaling methods are seldom used in the field of welding; one possible reason for this

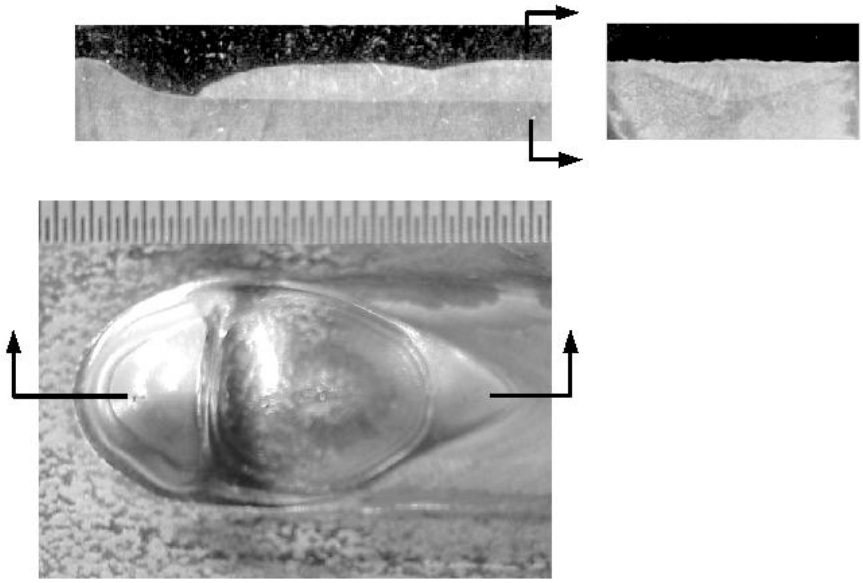

Figure 2: Weld pool at high currents and speeds (500 A, 35.4 ipm)

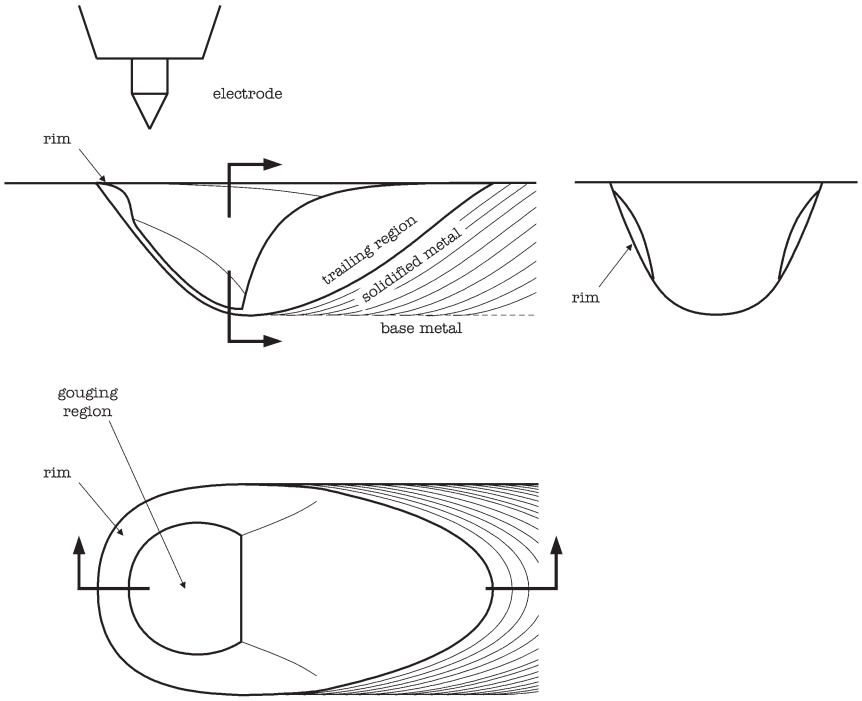

Figure 3: Schematic of the weld pool at high currents and speeds. The free surface is very depressed, turning into a thin liquid film under the arc. A thicker rim of liquid runs around the edge of the weld pool carrying molten metal to the bulk of liquid at the rear of the weld pool. The transition line marks the abrupt change from the thin liquid film into the bulk of liquid at the rear.

Table 1: Summary of relevant studies on weld pool depression. X=experimental, A=analytical, N=numerical. GTA=gas tungsten arc, GMA=gas metal arc, SMA=shielded metal arc, SA=submerged arc

Year	Author	Type	Meth.	Amp. max.	Remarks	Reference
1962	Ishizaki	GTA, SMA, SA	X	1200	gouging, traveling	[7, 15]
1968	Bradstreet	GMA	X	570	gouging, traveling	[1]
1972	Demyantsevich	GTA	X	530	gouging, traveling	[16]
1975	Shimada *et al.*	GTA	X, A	800	gouging, traveling	[2, 3]
1979	Matsunawa *et al.*	GMA	X, A	350	gouging, traveling	[17]
1992	Adonyi *et al.*	GTA	X	1000	gouging, traveling	[18]
1983	Lin *et al.*	GTA	X, A	600	spot weld	[19, 20, 21, 22]
1993	Rokhlin *et al.*	GTA	X, A	350	spot weld	[23]
1978	Friedman	GTA	N	125	spot weld	[10]
1989	Tsai *et al.*	GTA	N	≈150	spot weld	[24]
1989	Szekely *et al.*	GTA	N	150	spot weld	[25, 26, 27]
1991	Zacharia *et al.*	GTA	N	150	spot weld	[28, 29]
1992	Na *et al.*	GTA	N	300	spot weld	[14, 30, 31]
1988	Zacharia *et al.*	GTA	N	100	traveling weld	[12, 13]
1995	Kim *et al.*	GMA	N	300	traveling weld	[32]
1996	Weiss *et al.*	GMA	N	155	traveling weld	[9]
1997	Ushio *et al.*	GMA	N	250	traveling weld	[33]

is that the large number of dimensionless groups obtained through dimensional analysis make the selection of a proper scale extremely difficult. Oreper and Szekely[6] obtained scaling factors for the characteristic velocity in a weld pool with a flat surface dominated by Marangoni forces. Rivas and Ostrach[34] extended the scaling to regimes with higher Marangoni numbers. Chen[35] presented a study of scaling and asymptotic considerations in convective heat transfer where he stated that "real world" heat transfer problems are too complex for the basic non-dimensionalization schemes, and that scaling factors can be obtained from the governing differential equations. Barenblatt[36] used dimensional analysis to classify different types of asymptotic approximations. Denn[37] presented scaling factors for the pressure and time in process fluid mechanics.

The methodology presented here presents a systematic new way of combining dimensional analysis and asymptotic considerations. Dimensional analysis permits a formulation of the problem in a dimensionless form, thus reducing the number of arguments. The asymptotic considerations allow one to scale the problem with the dominant terms in the equations. A normalization procedure and functional requirements are clearly defined here; this way the procedure is mathematically sound, relying more on knowledge rather than intuition as in previous works. The outcome of the order of magnitude scaling methodology consists of estimations of the characteristic values of the solution of the problem, and a ranking of the relative importance of the different driving forces involved. The estimations obtained have only an order of magnitude accuracy, but they are very general and simple to obtain. They are obtained using matrix algebra, simplifying otherwise tedious algebraic manipulations prone to human error.

There are important differences between order of magnitude scaling and dimensional analysis. Dimensional analysis helps to reduce the number of arguments on which a given problem depends, but it provides no additional information about the solution of a problem; there is no information about the relative importance of the dimensionless groups involved. Order of magnitude scaling provides estimations of the solution, and determines the relative importance of the dimensionless groups. This is possible because this technique uses asymptotic techniques. The dimensionless functions that relate the exact solution to the estimations have a value of approximately one, and depend on the set of dimensionless groups determined through dimensional analysis. These functions can be determined through solution of the equations or through experiments (whether physical or numerical). Knowing which dimensionless groups are negligible allows one to simplify the functional dependence of the dimensionless functions. This simplification can be done without significantly affecting the accuracy of the predictions, yet greatly reducing the number of experimental points necessary for the characterization of the functions.

Three aspects of the order of magnitude scaling methodology are especially relevant, and will be described in more detail below. These aspects are: normalization, functional requirements, and asymptotic considerations.

Normalization

The solution of a problem consists of a set of scalar functions with dimensions that describe the properties of the system in question; for example, temperature as a function of position: $T(X, Z)$. These dimensional functions are determined by a set of differential equations that represent the physics governing the problem. The goal of the normalization is to transform these dimensional functions into dimensionless functions with an absolute value between zero

and one. This can be accomplished by the following relationships:

$$x_i = \frac{X_i - A_i}{B_i - A_i} \tag{1}$$

$$f(x_1 \dots x_i \dots x_v) = \pm \frac{F(X_1 \dots X_i \dots X_v) - F(\mathbf{A})}{|F(\mathbf{B})| - |F(\mathbf{A})|} \tag{2}$$

In equations 1 and 2, capital letters are used for functions and arguments with dimensions, and small case for their dimensionless counterpart. The same convention will be maintained throughout the paper. The domain for scaling is the region over which the functions that constitute the solution of the problem are going to be scaled; this domain is defined by $A_i \leq X_i \leq B_i$, where A_i and B_i are the extreme values of each independent argument X_i. The points **A** and **B** are the points in the domain of scaling where the function $F(X_1 \dots X_i \dots X_v)$ has a minimum and maximum absolute value respectively. When $F(\mathbf{A}) = 0$, $F_C = |F(\mathbf{B})| - |F(\mathbf{A})|$ is the characteristic value of F. When $F(\mathbf{A}) \neq 0$, F_C is the characteristic value of the variation of F. This concept applies similarly to the independent arguments. The characteristic values are defined positive, because when performing algebraic operations they might be raised to a non-integer power.

An important aspect of this normalization is that one or more of its elements (**A**, **B**, F(**A**), or F(**B**)) might be initially unknown. For example, in the scaling of a very depressed weld pool, the characteristic value of the velocity at the surface is initially unknown. From a dimensional analysis point of view, the introduction of unknown parameters increases the number of dimensionless groups, which might seem to add complexity to the problem. However, since the problem is completely defined by the parameters appearing in the system of equations, the additional dimensionless groups are redundant, and they can be used in combination with asymptotic considerations to estimate the value of the unknown characteristic values.

Functional Requirements

The order of magnitude scaling methodology presented here requires that the second derivatives of the dimensionless functions are of the order of one. This requirement is particular to this formulation, and it guarantees that the first derivatives of the dimensionless functions have an upper bound of the order of one. In some cases a lower bound of the absolute value of the maximum can also be established to be of the order of one, and these functions will be described as having an "order of magnitude of one" with the notation OM(1).

Although the solution of the differential equations is unknown (especially if they are non-linear), in practice, previous insight from experiments or mathematical modeling is generally available. This insight is usually sufficient for determining whether the functions are smooth enough, or if the domain can be split into smaller regions in which the second derivatives of the dimensionless functions are of the order of one. For many engineering problems division into only two subdomains will suffice.

The requirement of having second derivatives of the order of one is very important, because it permits one to extract an algebraic equation from a differential one. The algebraic equation provides an estimation of the characteristic values in a much simpler way than the differential equation. For example, the equation of conservation of mass in two dimensional flow is:

$$\frac{\partial U}{\partial X} + \frac{\partial V}{\partial Y} = 0 \tag{3}$$

Using the normalization relationships (equations 1 and 2) the functions and their arguments can be expressed as a set of scaling relationships:

$$X = X_{min} + X_C x \tag{4}$$

$$Y = Y_{min} + Y_C y \tag{5}$$

$$U(X,Y) = U_{min} + U_C u(x,y) \tag{6}$$

$$V(X,Y) = V_{min} + \widehat{V}_C v(x,y) \tag{7}$$

In this example the characteristic value V_C is assumed to be unknown, and its estimation is marked with a hat ($\widehat{V}_C$).

Equation 3 can therefore be normalized as:

$$\frac{\partial u}{\partial x} + N_1 \frac{\partial v}{\partial y} = 0 \tag{8}$$

where $N_1 = \widehat{V}_C X_C / U_C Y_C$. When $\partial u/\partial x$=OM(1), and $\partial v/\partial y$=OM(1) the dimensionless group N_1 must be approximately equal to one. The estimation $\widehat{V}_C$ can be calculated by solving the algebraic equation $N_1 = 1$. For problems that involve q estimations, q algebraic equations are obtained, and the estimations can be obtained using matrix algebra (equation 75).

Asymptotic Considerations

The normalization of equation 3 is trivial because it has only two terms, and the only possible way of obtaining a dimensionless group is to combine them. When an equation has more than two terms there are many ways to obtain dimensionless groups. The correct normalization is the one that normalizes all terms with the largest coefficient. This way the largest dimensionless coefficient has a value of one, and all others have a value of one or less. In the asymptotic limit there is a balancing term (that has the same order of magnitude of the dominant term), and the coefficients of the other non-dominant terms approach zero. The dimensionless coefficient of the balancing term can be assigned a value of one, same as the value of the dominant coefficient. Assigning a value to a balancing term generates an algebraic equation.

The determination of the dominant and balancing terms in a system of equations is an iterative process. A wrong assignment produces dimensionless coefficients larger than one; therefore, a new assumption of dominant and balancing forces needs to be made.

The process described above has some differences with the dominant balance technique described by Bender *et al.*[38]. In their formulation, after neglecting the small terms, the simplified differential equations need to be solved exactly. In the formulation used here, it is only necessary to determine the value of the dimensionless coefficients, without solving the differential equations.

FORMULATION OF THE PROBLEM

The problem of weld pool surface depression at high current and velocity is modeled here as two-dimensional, quasi-steady state. The choice of two-dimensional modeling is reasonable because the dominant force (gas shear on the free surface) acts mainly in the direction of motion; this approximation yields an upper bound for the thickness of the thin liquid film in the gouging region. The focus of the order of magnitude scaling is on the molten metal processes in the

weld pool. The properties of the arc, and the heat transfer in the solid (which determines penetration) are considered as known process inputs. The properties of the molten metal are considered constant. The melting interface is considered sharp, as in pure metals.

Figure 4 presents the coordinate system and other important elements for the analysis. For a stationary torch the substrate moves to the right with velocity U_∞. If the substrate is considered as stationary the torch moves to the left, leaving behind a trail of solidifying metal. The weld pool has two characteristic regions, one is very thin and occurs under the arc (the gouging region), and a trailing region which is thicker. This analysis concentrates on the gouging region, and has for a goal the determination of the dominant driving force that causes the weld pool to turn into a thin film.

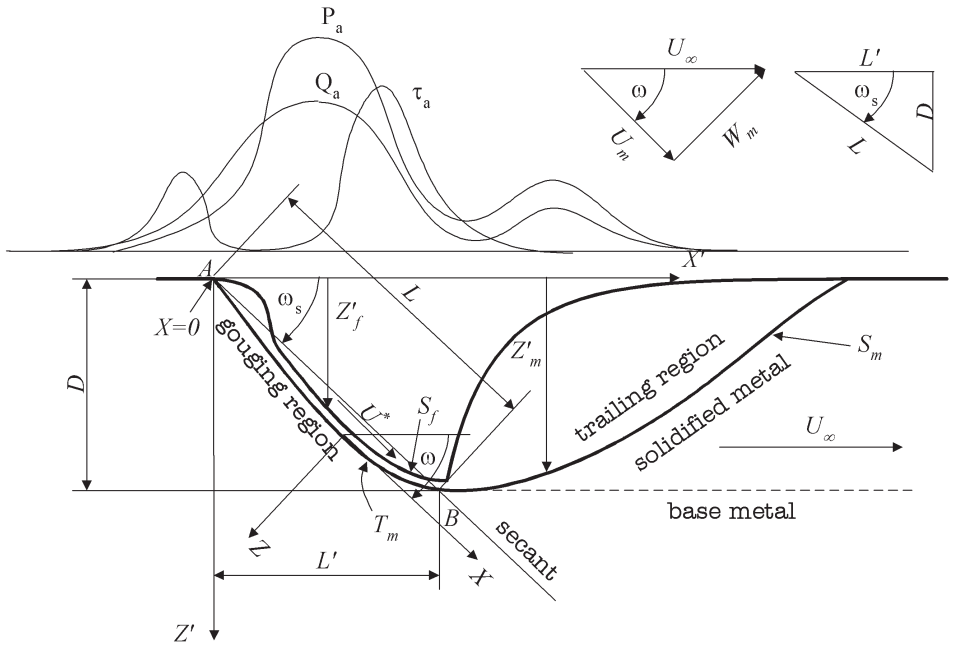

Figure 4: Coordinate system and other elements of a thin weld pool. The thickness of the thin liquid layer at point B is $\approx \widehat{\delta}$.

The curves labeled Q_a, P_a, and τ_a represent the heat input, arc pressure, and gas shear stress that the arc imposes on the free surface. S_f and S_m represent the free surface and the melting interface respectively. In this formulation of the problem S_m is considered as prescribed, and S_f as an unknown to be determined.

The reference axes travel with the welding torch so that the problem can be solved as a pseudo-stationary one. The axes X and Z are tangential and normal to the melting interface (S_m), therefore their angle ω with the horizontal (axis X') changes along the melting front. The derivatives with respect to ω can be neglected when using the scaling relationships because the thickness of the liquid film is much smaller than the radius of curvature of the melting front. This approach is very similar to the one used by Wei and Giedt in their study of keyhole formation in electron beam welding [39]. The melting front angle ω_s is the angle of a secant to the melting front between the point of beginning of melting (point A in Figure 4) and the transition point

where the trailing region begins (point B).

Governing Equations and Boundary Conditions

The equations that govern the transport processes of the molten metal are mass conservation (equation 9), Navier Stokes (equations 10 and 11), and conservation of energy (equation 12). The following driving forces are considered:

- Gas shear on the free surface
- Arc pressure
- Electromagnetic forces
- Hydrostatic pressure
- Capillary forces
- Marangoni forces
- Buoyancy forces

The equations that completely describe the problem are the equations of conservation of mass (equation 9), the equations of Navier-Stokes, (equations 10 and 11), and the equation of conservation of energy (equation 12). The equations for the determination of the electromagnetic forces are Ohm's law (equations 13 and 14), the equation of conservation of charge (equation 15), and Ampère's law (equations 16 and 17). In this two-dimensional system, the magnetic flux vector is perpendicular to the page at all times. Among the boundary conditions, equation 20 includes the Marangoni effect and the gas shear due to the arc plasma, and equation 22 includes the arc pressure and the capillary forces.

Equation 18 is an approximate integral expression of the mass conservation equation at the transition point (point B in Figure 4), which is located near the bottom of the weld pool, where the slope of the melting front (angle $\omega \approx 0$) is approximately horizontal. The integral equation of conservation of mass is redundant because mass conservation is already considered with a differential expression in equation 9; however, the integral expression will be useful later for determination of the estimations. The effect of frictional and Joule heating is not included in these equations; they are usually considered negligible in the literature.

$$\frac{\partial U}{\partial X} + \frac{\partial W}{\partial Z} = 0 \tag{9}$$

$$\begin{aligned} U\frac{\partial U}{\partial X} + W\frac{\partial U}{\partial Z} &= -\frac{1}{\rho}\frac{\partial P}{\partial X} + \nu\left(\frac{\partial^2 U}{\partial X^2} + \frac{\partial^2 U}{\partial Z^2}\right) + g\sin(\omega) - \\ &\quad -\frac{1}{\rho}J_Z B_Y - \beta g \sin(\omega)\,(T - T_m) \end{aligned} \tag{10}$$

$$\begin{aligned} U\frac{\partial W}{\partial X} + W\frac{\partial W}{\partial Z} &= -\frac{1}{\rho}\frac{\partial P}{\partial Z} + \nu\left(\frac{\partial^2 W}{\partial X^2} + \frac{\partial^2 W}{\partial Z^2}\right) + g\cos(\omega) + \\ &\quad +\frac{1}{\rho}J_X B_Y - \beta g \cos(\omega)\,(T - T_m) \end{aligned} \tag{11}$$

$$U\frac{\partial T}{\partial X}+W\frac{\partial T}{\partial Z} = \alpha\left(\frac{\partial^2 T}{\partial X^2}+\frac{\partial^2 T}{\partial Z^2}\right) \quad (12)$$

$$J_X = -\sigma_e\frac{\partial \Phi}{\partial X} \quad (13)$$

$$J_Z = -\sigma_e\frac{\partial \Phi}{\partial Z} \quad (14)$$

$$\frac{\partial^2 \Phi}{\partial X^2}+\frac{\partial^2 \Phi}{\partial Z^2} = 0 \quad (15)$$

$$\frac{\partial B_Y}{\partial Z} = -\mu_0 J_X \quad (16)$$

$$\frac{\partial B_Y}{\partial X} = \mu_0 J_Z \quad (17)$$

$$(U_\infty + C_1\widehat{U})\widehat{\delta} \approx U_\infty L\sin(\omega_s) \quad (18)$$

The expression of the constant C_1 in the integral equation of conservation of mass (equation 18) is:

$$C_1 = \frac{1}{U_C\delta_C}\int_0^{\delta_C}(U-U_\infty)dZ \quad (19)$$

where U_C and δ_C are the characteristic values of the velocity in $U(X,Y)$ and thickness of the thin liquid layer. Since these values are unknown, they are estimated by $\widehat{U}$ and $\widehat{\delta}$.

The constant C_1 represents the ratio between the average velocity and the free surface velocity for the liquid film at point B (Figure 4). For a flow dominated by viscous forces C_1 approaches $1/2$, and for a flow dominated by inertial forces (uniform velocity profile) C_1 approaches 1. In this work the value $C_1 = 1/2$ will be used, because (as it will be shown later) in a thin weld pool the flow is dominated by viscous forces.

Boundary conditions

Table 2: Boundary conditions for a thin weld pool (dimensional)

	U	W	P	T	Φ	δ	B_Y
S_f	Eq. 20, Eq. 21		Eq. 22	Eq. 23	Eq. 24		
S_m	U_m	W_m	Eq. 25	T_m			
$x=0$						0	
$x'=\pm\infty$					0		0
$z'=+\infty$					0		0

$$\sigma_T\nabla T\cdot\mathbf{e}_t = -\tau_a-\rho\nu\nabla(\mathbf{U}\cdot\mathbf{e}_t)\cdot\mathbf{e}_n \quad (20)$$

$$\mathbf{U} \cdot \mathbf{e}_n = 0 \tag{21}$$

$$P = \frac{\sigma \frac{d^2 Z_f'}{dX'^2}}{\left(1 + \left(\frac{dZ'}{dX'}\right)^2\right)^{3/2}} + P_a \tag{22}$$

$$k\frac{\partial T}{\partial Z} = -Q_a \tag{23}$$

$$\sigma_e \frac{\partial \Phi}{\partial Z} = -J_a \tag{24}$$

$$P = \rho g Z_m' \tag{25}$$

where U_m and W_m are the velocity of the metal at the melting interface, $\mathbf{U}$ is the velocity vector and $\mathbf{e}_X$, $\mathbf{e}_Z$, $\mathbf{e}_t$ and $\mathbf{e}_n$ are the unit vectors for the X and Z directions, tangential and normal to the free surface, as shown in Figure 5. The domain for scaling is $0 \leq X \leq L$ and $0 \leq Z \leq \delta_C$.

$$U_m = U_\infty \cos(\omega) \tag{26}$$

$$W_m = -U_\infty \sin(\omega) \tag{27}$$

$$\mathbf{U} = U\mathbf{e}_X + W\mathbf{e}_Z \tag{28}$$

$$\mathbf{e}_t = \cos(\gamma)\mathbf{e}_X - \sin(\gamma)\mathbf{e}_Z \tag{29}$$

$$\mathbf{e}_n = \sin(\gamma)\mathbf{e}_X + \cos(\gamma)\mathbf{e}_Z \tag{30}$$

$$\tan(\gamma) = \frac{d\delta}{dX} \tag{31}$$

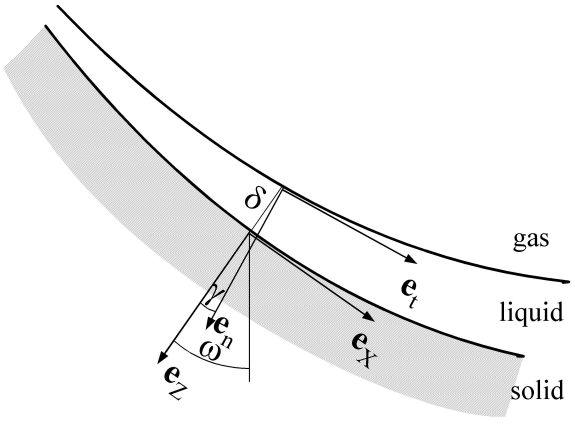

Figure 5: Coordinate vectors at the melting interface and free surface. The angle γ is small because the variations in thickness of the thin weld pool are smooth

Values for a typical case

A representative case will be used to determine relative importance of the driving forces of a typical weld pool with a deeply depressed surface. The main welding parameters for this case are shown in Table 3, and material properties can be found in Table 4.

The measured weld penetration and its location are:

$$\begin{aligned} D &= 3.2 \text{ mm} \\ L' &= 4.15 \text{ mm} \\ \omega_s &= 0.657 \text{ rad} \end{aligned}$$

Table 3: Welding parameters for a typical weld with a very depressed free surface

base material	AISI 304 (50 ppm S)
current	305 A
voltage	14.5 V
speed	12 ipm (5.08 mm/s)
arc length$_{flat}$	3.175 mm
shielding gas	100% Ar

No studies have been performed to determine the exact characteristics of the arc in deeply depressed weld pools. The peak values Q_{max}, P_{max}, J_{max}, and τ_{max} are estimated as similar to the values for an arc on a flat surface; the first three need a correction for the larger area of the inclined front surface:

$$Q_{max} \approx Q_{max,flat} \cos(\omega_s) \tag{32}$$

$$P_{max} \approx P_{max,flat} \cos(\omega_s) \tag{33}$$

$$J_{max} \approx J_{max,flat} \cos(\omega_s) \tag{34}$$

$$\tau_{max} \approx \tau_{max,flat} \tag{35}$$

The arc length must also be corrected for the weld pool depression:

$$\text{arc length} \approx \text{arc length}_{flat} + D/2 \tag{36}$$

These approximations are conservative because they underestimate the importance of the dominant driving force and overestimate the magnitude of the other forces. Since the melting front is inclined with respect to the arc axis, the gas shear stress in the gouging region is expected to be larger than over a perpendicular flat surface. The data for an arc on a flat surface is interpolated from the measurements by Tsai [40] and modeling by Choo [27]. The heat distribution between the gouging region and trailing region of the weld pool depends on the position of the transition line. As the current increases, the transition line moves towards the rear and less heat reaches the trailing region. At the onset of humping the arc energy is concentrated almost exclusively in the gouging region. For the representative settings of Table 3, the estimated parameters for the arc are:

$$Q_{max} = 3.34 \times 10^7 \text{ W/m}^2$$

$$
\begin{aligned}
P_{max} &= 713\,\mathrm{Pa} \\
J_{max} &= 4.29 \times 10^{6}\ \mathrm{A/m^2} \\
\tau_{max} &= 92.1\,\mathrm{Pa}
\end{aligned}
$$

Table 4: Physical properties for AISI 304 with 50 ppm S. This data is based on references [29, 31, 41, 42, 43, 44].

ρ	6907	kg/m^3	ν	8.32×10^{-7}	m^2/s
α	3.30×10^{-6}	m^2/s	σ_T	1.50×10^{-4}	N/mK
k	18.0	W/mK	σ	1.56	N/m
σ_e	7.7×10^{5}	A/Vm	β	9.79×10^{-5}	1/K
T_s	1523	K	T_l	1723	K

ORDER OF MAGNITUDE SCALING OF A THIN WELD POOL

Scaling Relationships

The equations below constitute the set of scaling relationships that transform dimensional functions into their dimensionless counterparts.

$$
\begin{aligned}
X &= Lx && (37)\\
X' &= L'x' && (38)\\
Z &= \widehat{\delta} z && (39)\\
\delta(X) &= \widehat{\delta}\Delta(x) && (40)\\
U(X,Z) &= U_m(\omega) + \widehat{U}u(x,z) && (41)\\
W(X,Z) &= W_m(\omega) + \widehat{W}w(x,z) && (42)\\
P(X,Z) &= \widehat{P}p(x,z) && (43)\\
T(X,Z) &= T_m + \widehat{T}\theta(x,z) && (44)\\
Z'_f(X') &= Dz'_f(x') && (45)\\
Z'_m(X') &= Dz'_m(x') && (46)\\
Q_a(X) &= Q_{max}q_a(x) && (47)\\
P_a(X) &= P_{max}p_a(x) && (48)\\
\tau_a(X) &= \tau_{max}t_a(x) && (49)\\
J_a(X) &= J_{max}j_a(x) && (50)\\
J_X(X,Z) &= \widehat{J}j_x(x,z) && (51)\\
J_Z(X,Z) &= J_{max}j_z(x,z) && (52)\\
B_Y(X,Z) &= \widehat{B}b(x,z) && (53)\\
\Phi(X,Z) &= \widehat{\Phi}\phi(x,z) && (54)
\end{aligned}
$$

Some of the characteristic parameters in the above relationships are not known and need to be estimated. These parameters constitute the set of estimations $\{S\}$. The goal of the order of magnitude scaling technique is to determine the expression of these estimations.

$$\{S\}^T = \{\widehat{\delta}, \widehat{U}, \widehat{W}, \widehat{P}, \widehat{T}, \widehat{\Phi}, \widehat{J}, \widehat{B}\}$$

Dimensionless Governing Equations and Boundary Conditions

Applying the scaling relationships (equations 37 to 54) to the governing equations (equations 9 to 25), a new set of equations involving dimensionless functions and arguments (but with dimensional coefficients) is obtained. This set of equations is normalized by using the modified dominant balance technique with the conditions and material properties of the typical case described above; this way a set of dimensionless equations is obtained (equations 55 to 73). The dominant balance determines that the gas shear and the viscous forces are dominant in a typical case (see Figure 8), and these will be the main forces used for the normalization. Equation 57 is normalized with the pressure gradient, which is characterized by equation 56. The expression of the dimensionless groups N_i is contained in the matrix $[A]$, shown in Figure 6. It contains the exponents of the different parameters and estimations in each dimensionless group. The internal lines divides matrix $[A]$ in six submatrices: $[A_{11}]$ to $[A_{23}]$. The exponents associated with the known parameters are contained in the three submatrices on the left ($[A_{11}]$, $[A_{21}]$, and $[A_{31}]$) and the unknown estimations on the three submatrices on the right ($[A_{12}]$, $[A_{22}]$, and $[A_{32}]$). The group on the top row ($[A_{11}]$ and $[A_{12}]$) includes the dimensionless groups that are assigned the value one. The middle row includes the dimensionless groups obtained through Buckingham's theorem[45]. The bottom row includes other dimensionless groups of unknown value that appear in the differential equations. For simplicity, elements with zero value are not represented in Figure 6.

$$\frac{\partial u}{\partial x} + N_1 \frac{\partial w}{\partial z} = 0 \tag{55}$$

$$N_2\left[(u_m + u)\frac{\partial u}{\partial x} + N_3(w_m + w)\frac{\partial u}{\partial z}\right] = -N_4\frac{\partial p}{\partial x} + N_5\frac{\partial^2 u}{\partial x^2} + \frac{\partial^2 u}{\partial z^2} - N_6\sin(\omega) - N_7 j_z b - N_8\sin(\omega) \tag{56}$$

$$N_9(u_m + u)\frac{\partial w}{\partial x} + N_{10}(w_m + w)\frac{\partial w}{\partial z} = -\frac{\partial p}{\partial z} + N_{11}\left(N_5\frac{\partial^2 w}{\partial x^2} + \frac{\partial^2 w}{\partial z^2}\right) + N_{12}\cos(\omega) + N_{13} j_x b - N_{14}\theta\cos(\omega) \tag{57}$$

$$N_{15}(u_m + u)\frac{\partial \theta}{\partial x} + N_16(w_m + w)\frac{\partial \theta}{\partial z} = N_5\frac{\partial^2 \theta}{\partial x^2} + \frac{\partial^2 \theta}{\partial z^2} \tag{58}$$

$$j_x = -N_{17}\frac{\partial \phi}{\partial x} \tag{59}$$

$$j_z = -N_{18}\frac{\partial \phi}{\partial z} \tag{60}$$

$$N_5\frac{\partial^2 \phi}{\partial x^2} + \frac{\partial^2 \phi}{\partial z^2} = 0 \tag{61}$$

$$\frac{\partial b}{\partial x} = -N_{20} j_z \tag{62}$$

$$\frac{N_{21}}{\sin(\omega_s)} + N_{22} \approx 1 \tag{63}$$

where:

$$u_m = N_{31} \cos(\omega) \tag{64}$$

$$w_m = -N_{32} \sin(\omega) \tag{65}$$

Boundary conditions

Table 5 presents the non-dimensional boundary conditions for this system. The conditions for the velocity at the surface have a complex mathematical expression, because the free surface is not necessarily parallel to the melting interface. Because the variation of film thickness over the length is smooth, equations 68 and 69 can contain the following simplifications:

$$\sin(\gamma) \approx \tan(\gamma) \tag{66}$$

$$\cos(\gamma) \approx 1 \tag{67}$$

Table 5: Boundary conditions for a thin weld pool (dimensionless)

	u	w	p	θ	ϕ	Δ	b
S_f	Eq. 68, Eq. 69		Eq. 70	Eq. 71	Eq. 72		
S_m	0	0	Eq. 73	0			
$x = 0$						0	
$x' = \pm\infty$					0		0
$z' = +\infty$					0		0

$$N_{23} \frac{\partial u}{\partial z} = -t_a - N_{24} \left(\frac{\partial \theta}{\partial x} + \frac{d\Delta}{dx} \frac{\partial \theta}{\partial z} \right) \tag{68}$$

$$w = N_{25}(u_m + u) \frac{d\Delta}{dx} - w_m \tag{69}$$

$$p = -N_{26} \frac{\sin(\omega_s)}{\cos^2(\omega_s)} \left(1 + \tan^2(\omega_s) \frac{dz'_f}{dx'} \right)^{-3/2} \frac{d^2 z'_f}{dx'^2} + N_{27} p_a \tag{70}$$

$$\frac{\partial \theta}{\partial z} = -N_{28} q_a \tag{71}$$

$$\frac{\partial \phi}{\partial z} = -N_{29} j_a \tag{72}$$

$$p = N_{30} z'_m \sin(\omega_s) \tag{73}$$

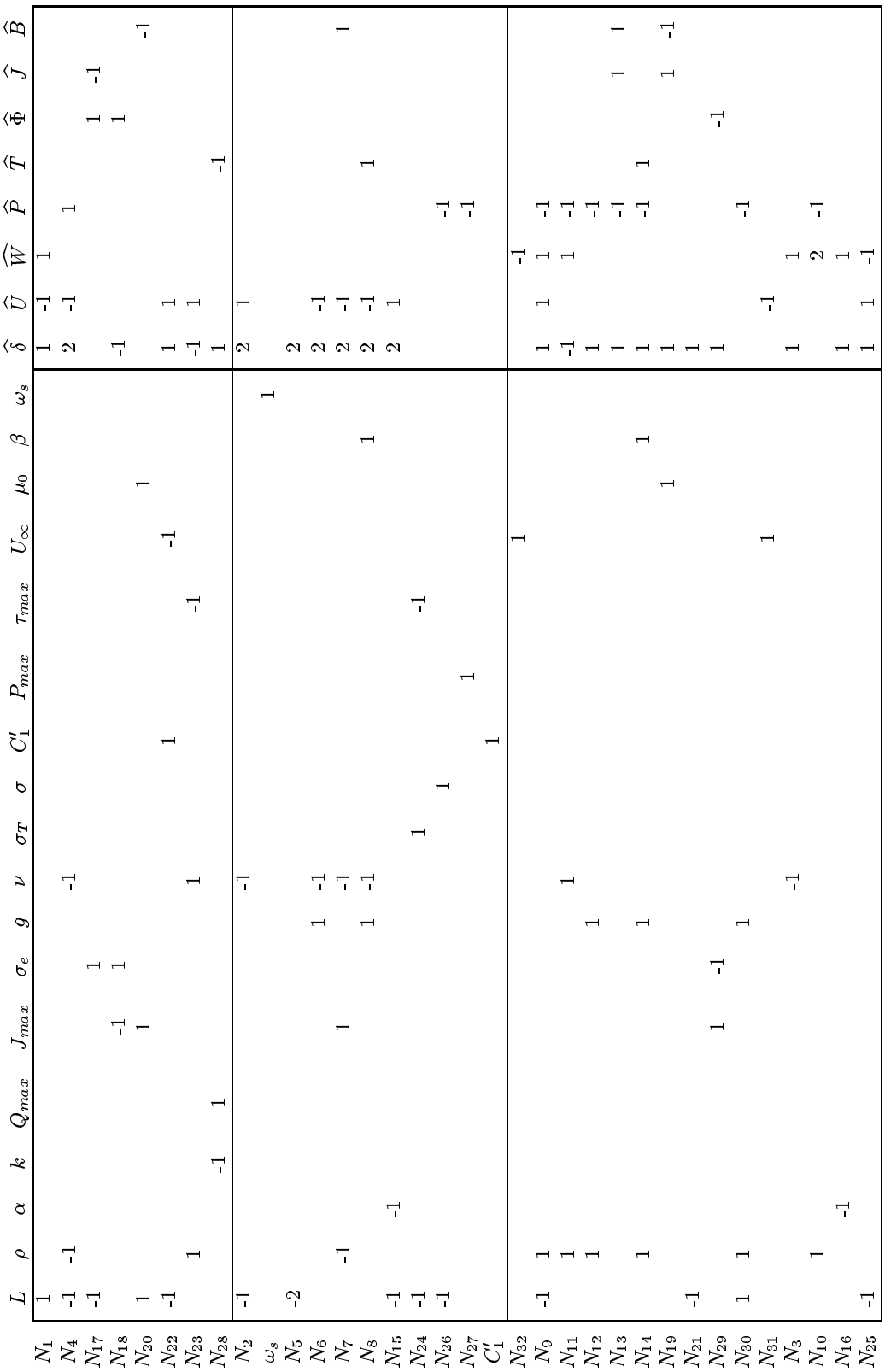

Figure 6: Matrix of dimensionless groups $[A]$ for a thin weld pool.

Dimensionless Groups of Known Order of Magnitude

The equations that have only two terms immediately yield dimensionless groups that can be estimated as equal to one; this way the following relationships are obtained:

$$N_1 = N_{17} = N_{18} = N_{20} = N_{28} = 1 \tag{74}$$

The main driving force (gas shear) acts mainly on the X direction. Therefore the momentum in X equation (equation 56) will be considered the most relevant of the two momentum equations. The characteristic pressure is obtained by defining $N_4 = 1$ in that equation. The dominant balance indicates that the gas shear at the surface is balanced by the viscous forces, therefore in equation 68 the group N_{23} should be set to one. For a thin liquid film the group N_{22} in the integral equation of conservation of mass (equation 63) dominates, and will be estimated as equal to one (this is valid only when the weld pool is very thin relative to its other dimensions).

Dimensionless Groups that Completely Describe the Problem

Eleven dimensionless groups are necessary to describe the non-dimensional formulation of the problem. The selection of these parameters is arbitrary, and for this problem the following set is chosen:

$$\{\Pi\} = \{N_2, \omega_s, N_5, N_6, N_7, N_8, N_{15}, N_{24}, N_{26}, N_{27}, C_1'\}$$

The elements of $\{\Pi\}$ have a concrete physical meaning, and many can be associated with well known dimensionless groups, as shown in Table 6. The parameters N_6, N_7, N_8, N_{24}, N_{26}, and N_{27}, are ratios of driving forces for the flow. The groups N_2, N_5, and N_{15}, are ratios of effects. ω_s relates to the geometry. The element C_1' is a numerical constant that is included in the set only for practical reasons. The term "diffusivity" used to describe N_5 refers to diffusion-like processes such as heat conduction or momentum transfer.

Table 6: Meaning of the governing dimensionless groups

	physical meaning	related group [46]
N_2	inertia/viscous	Reynolds
ω_s	melting front angle	see Figure 4
N_5	diffusivity in x/diffusivity in z	
N_6	gravity/viscous	Stokes
N_7	electromagnetic/viscous	Elsasser
N_8	buoyancy/viscous	Grashoff
N_{15}	convection/conduction	Peclet
N_{24}	Marangoni/gas shear	Marangoni
N_{26}	capillary/viscous	Capillary
N_{27}	arc pressure/viscous	Poiseuille

One advantage of the governing dimensionless numbers used here is that the ratios they represent describe the relative importance of driving forces or effects with an order of magnitude accuracy. The reason for this improved accuracy over standard dimensionless numbers is that the groups used here include information about characteristics of the problem that is not easily captured by the traditional formulation of dimensionless groups.

Expression of the Order of Magnitude Estimations

The expression of the order of magnitude estimations is given by matrix $[A_S]$, shown in Figure 7. This matrix is obtained from equation 75[47].

$$[A_S] = -[A_{12}]^{-1}[A_{11}] \tag{75}$$

	L	ρ	α	k	Q_{max}	J_{max}	σ_e	g	ν	σ_T	σ	C_1'	P_{max}	τ_{max}	U_∞	μ_0	β	ω_s
$\widehat{\delta}$	1/2	1/2							1/2			-1/2		-1/2	1/2			
$\widehat{U}$	1/2	-1/2							-1/2			-1/2		1/2	1/2			
$\widehat{W}$												-1			1			
$\widehat{P}$	1/2	-1/2							-1/2			1/2		3/2	-1/2			
$\widehat{T}$	1/2	1/2		-1	1				1/2			-1/2		-1/2	1/2			
$\widehat{\Phi}$	1/2	1/2				1	-1		1/2			-1/2		-1/2	1/2			
$\widehat{J}$	-1/2	1/2				1			1/2			-1/2		-1/2	1/2			
$\widehat{B}$	1					1										1		

Figure 7: Matrix of dimensionless groups $[A_S]$ for a thin weld pool.

The expressions in the form of equations for the characteristic thickness, surface velocity and temperature variation are the following:

$$\widehat{\delta} = (2\mu U_\infty D/\tau_{max})^{1/2} \tag{76}$$

$$\widehat{T} = Q_{max}\widehat{\delta}/k \tag{77}$$

$$\widehat{U} = 2U_\infty D/\widehat{\delta} \tag{78}$$

RESULTS

The value of the estimations obtained using order of magnitude scaling are presented in Table 7. The characteristic thickness for the liquid film is on the order of tens of microns, which is orders of magnitude smaller than the thickness for a weld pool with recirculation (of the order of millimeters). On such a thin weld pool, the characteristic temperature variation is of the order of 10^2 K, much smaller than that for weld pools with recirculation (of the order of 10^3 K). This smaller temperature jump makes Marangoni forces less relevant. Thus, variations in the sulfur content are expected to have a much smaller influence on penetration than in thicker weld pools.

Table 7: Typical values for the estimations in a thin weld pool

$\widehat{\delta}$	4.51×10^{-5}	m	$\widehat{T}$	83.8	K
$\widehat{U}$	0.722	m/s	$\widehat{\Phi}$	2.51×10^{-4}	V
$\widehat{W}$	6.20×10^{-3}	m/s	$\widehat{J}$	3.69×10^{4}	A/m^2
$\widehat{P}$	1.07×10^{4}	Pa	$\widehat{B}$	2.83×10^{-2}	Wb/m^2

The typical values for the dimensionless groups that describe the problem are shown in Figure 8. The value 1 corresponds to the ratio between the the gas shear force (dominant), and

viscous forces (balancing). An analysis of the groups related to the driving forces shows that their influence is smaller than 10% of the dominant force. Group $N_2 \approx 0.34$ is the ratio between two balancing forces (viscous and dynamic). Its value indicates that inertial forces should be taken into account in more accurate calculations. The very small value of N_5 indicates that in the X-direction thermal conduction and viscous effects are negligible. Convection (N_{15}) is also small.

The thickness of the mushy zone can be estimated as:

$$\text{thickness mushy zone} \approx kT_{sl}/Q_{max} = 1.07 \times 10^{-4}\,\text{m} \tag{79}$$

The typical weld pool has a thickness of the same order, and will capture the irregularities in the melting of the base metal, thus giving the impression of a "dry" surface.

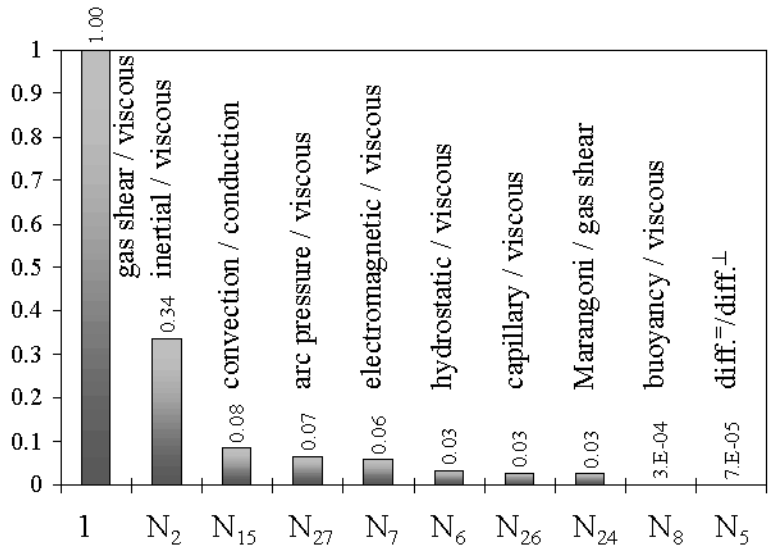

Figure 8: Typical value of the governing dimensional groups for a thin weld pool. The gas shear on the free surface is the dominant driving force, and viscosity is the dominant resistance (effect). All other forces and effects are normalized by them. In the asymptotic case when all other forces and effects are negligible, the ratio of gas shear/viscous effect is one. For the typical case presented, gas shear is an order of magnitude stronger than any other force. The viscous forces are the dominant resistance, but inertial effects are not negligible.

Experimental Evidence

In weld pools with recirculation Marangoni forces are dominant, and the presence of surface active elements such as sulfur[43] generates welds with significantly different penetration[5, 6]. GTA welds with a sulfur content of more than 70 ppm tend to be deeper and narrower than those with less than 60 ppm[48].

To verify that in a thin weld pool the Marangoni forces are of little importance, a set of bead on plate welds was performed in the same conditions on 304 stainless steel differing only on their sulfur content (6 ppm vs. 230 ppm). The welding parameters used in the experiments

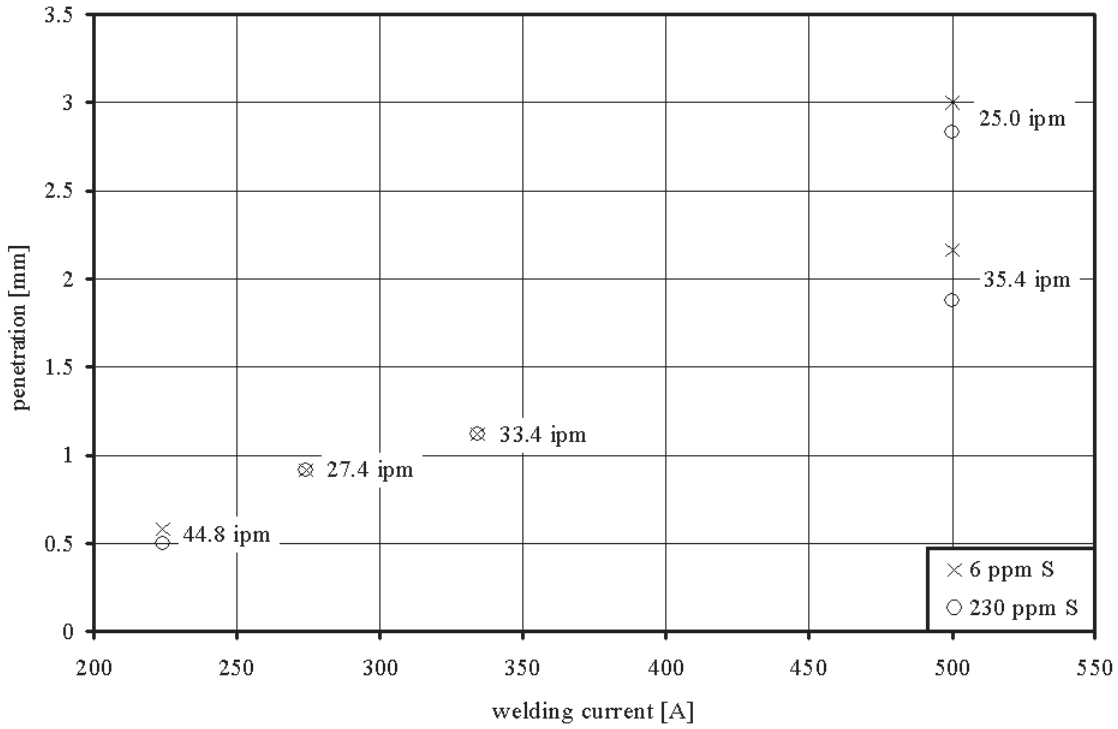

Figure 9: Welding penetration at high current. It can be observed that welding penetration varies very little with sulfur content, indicating that Marangoni forces are not dominant in this regime.

were such that these welds had a gouging region. The resulting welds were sectioned and etched, and penetration was measured. The results are shown in Figure 9. Welding penetration does not change significantly with the sulfur content, indicating that the Marangoni forces are of little effect at these high current levels.

DISCUSSION

Order of magnitude scaling indicates that the dominant force driving the flow and determining the position of the free surface in a very depressed weld pool is the gas shear on the surface. This was suggested before by Ishizaki[7] and Choo[8]. Based on experimental observations and physical modeling, Ishizaki proposed that the plasma shear pushed the fluid flow to the rear. Choo and Szekely performed numerical simulations of the arc and the weld pool for GTAW; they came to the conclusion that above 200 A the weld pool is likely to deform, and the gas shear could become dominant, although they could not study that case explicitly. Shimada *et al.*[3] measured the thickness of a solidified thin weld pool, obtaining a value of 70 μm, which is of the same order of magnitude as the estimations obtained here.

In the past, other forces have been considered likely candidates to be the driving force in a weld pool under high current (Electromagnetic forces, arc pressure, and Marangoni forces). A review of the literature indicates that electromagnetic forces and arc pressure cannot be the cause of the deep weld pool surface depressions observed experimentally. Tsai *et al.*[24]

indicated that the electromagnetic forces tend to raise the center of the weld pool, therefore they cannot be the cause for the depression. Lin *et al.*[20] and Rokhlin *et al.*[23] determined that at high currents (above approximately 250 A) the free surface deformation is of the order of five times that obtained from a balance between arc force and capillary and hydrostatic forces. The experiments performed in this research also discard Marangoni forces as the cause of weld pool surface depression at high currents.

Two dimensional modeling of the problem yields an upper bound for the thickness weld pool when it turns into a thin liquid film. The material that flows from the melting front to the rear through the rim (see Figure 3) is material that does not actually contribute to the film thickness. The gas flow on the surface is not perfectly parallel, and has an outward component, which also subtracts material from the thin weld pool. The behavior of the arc in a deeply depressed weld pool is not well known, and the values employed are those corresponding to a flat surface, with a correction related to the larger area of an inclined surface. This also results in an upper bound for the weld pool thickness, since the impingement of the arc over an inclined surface is expected to cause stronger shear stresses than when the arc axis is normal to a flat plate.

For the normalization of the governing equations, it was assumed that the layer thickness is much smaller than the radius of curvature of the melting front. This assumption is reasonable, in the light of the results obtained, since the thickness of the thin liquid film is of the order of magnitude of 10^{-5}m in a weld pool with characteristic dimensions of the order of 10^{-3}m.

The application of order of magnitude scaling to the analysis of this problem yielded approximate estimations of the characteristic values of the problem. The relationship between these estimations and the exact solutions depends on the set of dimensionless parameters resulting from the application of Buckingham's theorem, as indicated in equation 80 for the thickness of a thin weld pool. In this equation the dimensionless groups N_i represent ratios of forces as indicated in Figure 8, and ω_s is a dimensionless group related to the geometry of the problem.

$$\delta = \widehat{\delta} f(N_2, \omega_s, N_5, N_6, N_7, N_8, N_{15}, N_{24}, N_{26}, N_{27}) \tag{80}$$

Since most of these groups are very small, as indicated in Figure 8, equation 80 can be simplified to

$$\delta \approx \widehat{\delta} f(N_2, \omega_s) \tag{81}$$

The simplification of equation 81 facilitates significantly the empirical determination of the function f. Many fewer experiments (whether physical or numerical) are necessary to characterize a function with two arguments than one with ten.

SUMMARY

For thin weld pools under high current arcs, the gas shear stress is the main determinant of the motion of the liquid under the arc. Other factors such as Marangoni, electromagnetic and buoyancy have a much smaller effect.

The characteristic thickness, surface velocity and temperature under the arc can be evaluated with the following expressions (typical values are in parenthesis):

$$\begin{aligned} \widehat{\delta} &= (2\mu U_\infty D/\tau_{max})^{1/2} && (\approx 50\,\mu\text{m}) \\ \widehat{T} &= Q_{max}\widehat{\delta}/k && (\approx 100\,\text{K}) \\ \widehat{U} &= 2U_\infty D/\widehat{\delta} && (\approx 1\,\text{m/s}) \end{aligned}$$

The freezing time for the thin film is very small, and premature freezing can start a humped bead.

The thickness of the weld pool is of the order of the mushy zone, therefore the free surface captures its irregularities and has the appearance of "dry" metal.

Finger-like penetration in GTA welding can be explained as a combination of the deep penetration caused by the direct action of the arc on the melting front, and a widening of the bead by the hot metal of the tail. Since the Marangoni forces are small relative to aerodynamic drag, surface active elements such as sulfur have a negligible effect on penetration.

A more accurate estimation of the characteristics of the arc in deeply depressed weld pools is necessary. This is especially important for the calculation of penetration, because on such thin weld pools the arc acts almost directly over the melting interface.

In the light of the results obtained, some conclusions can be drawn upon the methodology used. Order of magnitude scaling provides scaling factors of the same order of magnitude as the unknowns; therefore, when normalizing the functions with these factors, the dimensionless functions obtained are smooth, and with values not far from unity. These dimensionless functions depend on a set of dimensionless groups as indicated by Buckingham's theorem of dimensional analysis[45]; however, order of magnitude scaling can go beyond dimensional analysis by helping to determine which of those dimensionless groups can be neglected.

Solutions obtained through numerical methods can be generalized by normalization with the proper scaling factors. This is also valid for experimental results. The scaling factors obtained can be used as a check for numerical results, as used by Oreper and Szekely[6], Thompson and Szekely[25], and Rivas and Ostrach[34].

The estimations obtained can be refined by further calculations or experiments. The knowledge gained regarding what dimensionless groups can be neglected reduces significantly the necessary number of experiments or calculations. The simple expression of the solutions makes them suitable to be implemented in real-time control algorithms. When using matrix algebra to implement this methodology, the matrices involved are generally small, and the matrix operations are relatively simple.

ACKNOWLEDGMENTS

This work was supported by the United States Department of Energy, Office of Basic Energy Sciences.

LIST OF SYMBOLS

b	dimensionless magnetic flux
$\widehat{B}$	estimation of characteristic magnetic flux
B_y	magnetic flux
C_1	mass conservation constant
D	weld penetration
g	gravity
$\widehat{J}$	estimation of characteristic current density
j_a	dimensionless current density at the surface
J_a	current density at the surface
J_{max}	maximum current density at the surface

j_x	dimensionless current density in x
J_x	current density in X
j_z	dimensionless current density in z
J_z	current density in Z
k	liquid heat conductivity
L	characteristic length in X
L'	characteristic length in X'
p	dimensionless pressure
P	pressure
$\widehat{P}$	estimation of characteristic pressure
p_a	dimensionless pressure at the surface
P_a	pressure at the surface
P_{max}	maximum pressure at the surface
q_a	dimensionless heat flux at the surface
Q_a	heat flux at the surface
Q_{max}	maximum heat flux at the surface
T	temperature
$\widehat{T}$	estimated characteristic temperature variation
T_l	liquidus temperature
T_s	solidus temperature
t_a	dimensionless gas shear stress at the surface
T_m	melting temperature
u	dimensionless velocity in x
U	velocity in X
$\widehat{U}$	estimated characteristic velocity in X
u_m	dimensionless base material in x
U_m	base material velocity in X
U_∞	welding velocity
w	dimensionless velocity in z
W	velocity in Z
$\widehat{W}$	estimated characteristic velocity in Z
w_m	dimensionless base material velocity in z
W_m	base material velocity in Z
${z_f}'$	dimensionless free surface position
${Z_f}'$	free surface position
${z_m}'$	dimensionless melting interface position
${Z_m}'$	melting interface position

Greek Symbols

α	liquid heat diffusivity
β	volumetric thermal expansion
$\widehat{\delta}$	estimated characteristic thickness of liquid film
Φ	electric potential
$\widehat{\Phi}$	estimated characteristic electric potential
ϕ	dimensionless electric potential

μ	viscosity
μ_0	magnetic permeability of vacuum
ν	kinematic viscosity
Π_i	governing dimensionless groups
θ	dimensionless temperature
ρ	liquid density
σ	surface tension
σ_e	electrical conductivity
σ_T	surface tension temperature coefficient
τ_a	gas shear stress at the surface
τ_{max}	maximum gas shear stress at the surface
ω	angle between tangent of melting front and horizontal
ω_0	angle between secant of melting front and horizontal

References

[1] B. J. Bradstreet. Effect of Surface Tension and Metal Flow on Weld Bead Formation. *Weld. J.*, pages 314s–322s, 1968.

[2] T. Yamamoto and W. Shimada. A Study on Bead Formation in High Speed TIG Arc Welding. In *International Symposium in Welding*, Osaka, Japan, 1975.

[3] W. Shimada and S. Hoshinouchi. A Study on Bead Formation by Low Pressure TIG Arc and Prevention of Under-Cut Bead. *Quart. J. Japan Weld. Soc.*, 51(3):280–286, 1982.

[4] W. F. Savage, E. F. Nippes, and K. Agusa. Effect of Arc Force on Defect Formation in GTA Welding. *Weld. J.*, pages 212s–224s, 1979.

[5] C. R. Heiple and J. R. Roper. Mechanism for Minor Element Effect on GTA Fusion Zone Geometry. *Weld. J.*, pages 97s–102s, 1982.

[6] G. M. Oreper and J. Szekely. Heat and Fluid Flow Phenomena in Weld Pools. *J. Fluid Mech.*, 147:53–79, 1984.

[7] K. Ishizaki. Interfacial Tension Theory of the Phenomena of Arc Welding - Mechanism of Penetration. In *Physics of the Welding Arc*, pages 195–209, London, UK, 1962. The Institute of Welding.

[8] R. T. C. Choo and J. Szekely. The Effect of Gas Shear Stress on Marangoni Flows in Arc Welding. *Weld. J.*, pages 223s–233s, 1991.

[9] D. Weiss, U. Franz, and J. Schmidt. Simulation of Weld Pool Formation During Vertical Arc Welding with Emphasis on the Influence of Groove Preparation. In *Computer Technology in Welding*, page Paper 36, Lanaken, Belgium, 1996. The Welding Institute.

[10] E. Friedman. Analysis of Weld Puddle Distortion and Its Effect on Penetration. *Weld. J.*, pages 161s–166s, 1978.

[11] G. M. Oreper, T. W. Eagar, and J. Szekely. Convection in Arc Weld Pools. *Weld. J.*, pages 307s–312s, 1983.

[12] T. Zacharia, A. H. Eraslan, and D. K. Aidun. Modeling of Non-Autogenous Welding. *Weld. J.*, pages 18s–27s, 1988.

[13] T. Zacharia, A. H. Eraslan, and D. K. Aidun. Modeling of Autogenous Welding. *Weld. J.*, pages 53s–62s, 1988.

[14] S.-D. Kim and S.-J. Na. Effect of Weld Pool Deformation on Weld Penetration in Stationary Gas Tungsten Arc Welding. *Weld. J.*, pages 179s–193s, 1992.

[15] K. Ishizaki. A New Approach to the Mechanism of Penetration. In N. Bailey, editor, *Weld Pool Chemistry and Metallurgy*, volume 1, pages 65–76, London, UK, 1980. The Welding Institute.

[16] V. P. Demyantsevich and V. D. Matyukhin. Characteristics of the Movement of Molten Metal in the Weld Pool During Welding with a Non-Consumable Electrode. *Svar. Proiz.*, (10):1–3, 1972.

[17] A. Matsunawa and K. Nishiguchi. Arc Behaviour, Plate Melting, and Pressure Balance of the Molten Pool in Narrow Grooves. In W. Lucas, editor, *Arc Physics and Weld Pool Behaviour*, volume 1, pages 301–310, London, UK, 1979. The Welding Institute.

[18] Y. Adonyi, R. W. Richardson, and W. A. Baeslack III. Investigation of Arc Effects in Subsurface GTA Welding. *Weld. J.*, pages 321s–330s, 1992.

[19] M. L. Lin and T. W. Eagar. Influence of Surface Depression and Convection on Arc Weld Pool Geometry. In *Transport Phenomena in Materials Processing*, volume 10, pages 63–69. ASME, 1983.

[20] M. L. Lin and T. W. Eagar. Influence of Arc Pressure on Weld Pool Geometry. *Weld. J.*, pages 163s–169s, 1985.

[21] M. L. Lin. *Transport Process Affecting the Shape of Arc Welds.* Doctor of Philosophy, Massachusetts Institute of Technology, 1985.

[22] M. L. Lin and T. W. Eagar. Effects of Surface Depression and Convection in GTA Welding. In S. A. David, editor, *International Conference on Trends in Welding Research*, Advances in Welding Science and Technology, pages 47–51, Gatlinburg, TN, 1986. ASM International.

[23] S. I. Rokhlin and A. C. Guu. A Study of Arc Force, Pool Depression, and Weld Penetration During Gas Tungsten Arc Welding. *Weld. J.*, pages 381s–390s, 1993.

[24] M. C. Tsai and S. Kou. Marangoni Convection in Weld Pools with a Free Surface. *Int. J. Num. Meth. Fluids*, 9:1503–1516, 1989.

[25] M. E. Thompson and J. Szekely. The Transient Behaviour of Weldpools with a Deformed Free Surface. *Int. J. Heat Mass Transfer*, 32(6):1007–1019, 1989.

[26] R. T. C. Choo, J. Szekely, and R. C. Westhoff. Modelling of High Current Arcs in Welding with Emphasis on Free Surface Phenomena in Weldpool. *Weld. J.*, 69(9):346s–361s, 1990.

[27] R. T. C. Choo. *Mathematical Modelling of Heat and Fluid Flow Phenomena in a Mutually Coupled Welding Arc and Weld Pool.* Doctor of Science, Massachusetts Institute of Technology, 1991.

[28] T. Zacharia, S. A. David, J. M. Vitek, and H. G. Kraus. Computational Modeling of Stationary Gas-Tungsten-Arc Weld Pools and Comparison to Stainles Steel 304 Experimental Results. *Met. Trans. B*, 22B:243–257, 1991.

[29] T. Zacharia and S. A. David. Heat and Fluid Flow in Welding. In *Mathematical Modelling of Weld Phenomena*, pages 3–23. 1992.

[30] W.-H. Kim, H. G. Fan, and S.-J. Na. A Mathematical Model of Gas Tungsten Arc Welding Considering the Cathode and the Free Surface of the Weld Pool. *Met. Mat. Trans. B*, 28B:679–686, 1997.

[31] S.-Y. Lee and S.-J. Na. A Numerical Analysis of Molten Pool Convection Considering Geometric Parameters of Cathode and Anode. *Weld. J.*, pages 484s–497s, 1997.

[32] J.-W. Kim and S.-J. Na. A Study on the Effect of Contact Tube-to-Workpiece Distance on Weld Pool Shape in Gas Metal Arc Welding. *Weld. J.*, pages 141s–151s, 1995.

[33] M. Ushio and C. S. Wu. Matematical Modeling of Three-Dimensional Heat and Fluid Flow in a Moving Gas Metal Arc Weld Pool. *Met. Mat. Trans. B*, 28B:509–516, 1997.

[34] D. Rivas and S. Ostrach. Scaling of Low-Prandtl-Number Thermocapillary Flows. *Int. J. Heat Mass Transfer*, 35(6):1469–1479, 1992.

[35] W.-K. Chen. Algebraic Theory of Dimensional Analysis. *Journal of the Franklin Institute*, 292(6):403–422, 1971.

[36] G. I. Barenblatt. *Scaling, self-similarity, and intermediate asymptotics.* Cambridge texts in applied mathematics ; 14. Cambridge University Press, New York, 1996.

[37] M. M. Denn. *Process Fluid Mechanics.* Prentice-Hall International Series in the Physical and Chemical Engineering Series. Prentice-Hall, Englewood Cliffs, NJ, first edition, 1980.

[38] C. M. Bender and S. A. Orszag. *Advanced Mathematical Methods for Scientists and Engineers.* International series in pure and applied mathematics. McGraw-Hill, New York, 1978.

[39] P. S. Wei and W. H. Giedt. Surface Tension Gradient-Driven Flow Around an Electron Beam Welding Cavity. *Weld. J.*, pages 251s–259s, 1985.

[40] N.-S. Tsai. *Heat Distribution and Weld Bead Geometry in Arc Welding.* Doctor of Philosophy, Massachusetts Institute of Technology, 1983.

[41] Y. Chen, S. A. David, and T. Zacharia. Arc-Pool Interaction and its Effects on the Development of the Weld pool. Submitted for publication at the Welding Journal, Oak Ridge National Laboratory, 1997.

[42] R. T. C. Choo, J. Szekely, and S. A. David. On the Calculation of the Free Surface Temperature of Gas-Tungsten-Arc Weld Pools from First Principles: Part II. Modeling the Weld Pool and Comparison with Experiments. *Met. Trans. B*, 23B:371–384, 1992.

[43] P. Sahoo, T. DebRoy, and M. J. McNallan. Surface Tension of Binary Metal-Surface Active solute Systems under Conditions Relevant to Welding Metallurgy. *Met. Trans. B*, 19B:483–491, 1988.

[44] K. W. Mahin, A. B. Shapiro, and J. Hallquist. Assessment of boundary Condition Limitations on the Development of a General Computer Model for Fusion Welding. In S. A. David, editor, *International Conference on Trends in Welding Research*, Advances in Welding Science and Technology, pages 215–223, Gatlinburg, TN, 1986. ASM International.

[45] E. Buckingham. On Physically Similar Systems; Illustrations of the Use of Dimensional Equations. *Phys. Rev.*, 4(4):345–376, 1914.

[46] Omega Engineering Inc. Chart of Dimensionless Numbers, 1995.

[47] P. F. Mendez. Doctor of Philosophy, Massachusetts Institute of Technology, 1999.

[48] K. C. Mills and B. J. Keene. Factors Affecting Variable Weld Penetration. *Int. Materials Rev.*, 35(4):185–216, 1990.